frontiers | Frontiers in Marine Science

TYPE Original Research
PUBLISHED 11 April 2024
DOI 10.3389/fmars.2024.1385517

OPEN ACCESS

EDITED BY
Chengji Shen,
Hohai University, China

REVIEWED BY
Zhang Bo,
Shandong University of Science and Technology, China
Qingzhi Zhu,
Stony Brook University, United States
Kai Xiao,
Southern University of Science and Technology, China

*CORRESPONDENCE
Wenran Cao
wenran.cao@uqconnect.edu.au
Guanxi Yan
g.yan@uq.edu.au

RECEIVED 13 February 2024
ACCEPTED 26 March 2024
PUBLISHED 11 April 2024

CITATION
Cao W, Hofmann H, Yan G and Scheuermann A (2024) Porewater exchange and iron transformation in a coastal groundwater system: a field investigation, driving mechanisms analysis, and conceptual model.
Front. Mar. Sci. 11:1385517.
doi: 10.3389/fmars.2024.1385517

Porewater exchange and iron transformation in a coastal groundwater system: a field investigation, driving mechanisms analysis, and conceptual model

Wenran Cao[1]*, Harald Hofmann[2,3], Guanxi Yan[1]* and Alexander Scheuermann[1]

[1]School of Civil Engineering, University of Queensland, St. Lucia, QLD, Australia, [2]School of the Environment, University of Queensland, St. Lucia, QLD, Australia, [3]Environment, Commonwealth Scientific and Industrial Research Organisation (CSIRO), Dutton Park, QLD, Australia

The high concentration of dissolved iron (Fe) in coastal waters triggers Lyngbya blooms in the Moreton Bay region of Southeast Queensland, Australia. Previous studies have provided a restricted understanding of how land-derived Fe is transported and then transformed into other forms (e.g., Fe oxides) before its release into the ocean. Here, a field investigation was conducted at a sandy beach on the northern end of Deception Bay, Queensland, Australia, focusing on porewater exchange and Fe transformation. This study revealed that tides provided a significant mechanism for driving the groundwater-seawater mixing in the intertidal area. Such forcing formed an upper saline plume (USP) with high dissolved oxygen (DO), creating a dynamic reaction zone for Fe oxidation and precipitation beneath the USP. The spatial distribution of Fe oxides highlighted a substantial Fe content in the subsurface, providing concrete evidence for the transformation of Fe from an aqueous state to a solid form. It also exhibited a low-permeable area that served as a geochemical barrier, absorbing chemical components like phosphate. These findings can assist in constructing a more accurate transport model that couples physical and geochemical processes to quantify the mechanisms driving Fe transformation in coastal areas and further deepen our comprehension of the hydrogeochemical functionalities in land-ocean connectivity via groundwater.

KEYWORDS

coastal groundwater system, field investigation, groundwater-seawater mixing, Fe(II) and Fe(III), dissolved oxygen (DO), porewater and sediment

1 Introduction

In recent decades, there has been an increasing recognition that submarine groundwater discharge (SGD) is a significant pathway for transporting solutes from land to the ocean (Moore, 2003; Robinson et al., 2007; Xin et al., 2010; Liu et al., 2016; Shen et al., 2018; Russo et al., 2023). The movement of fresh groundwater from land to the ocean prevents seawater intrusion and creates two distinct zones in the intertidal area. One of those is the saltwater wedge (SW), traditionally recognized as the primary area where groundwater and seawater mix (Charette and Sholkovitz, 2002; Ullman et al., 2003; Miller and Ullman, 2004; Slomp and Van Cappellen, 2004; Zipperle and Reise, 2005); the other is the upper saline plume (USP), a surficial mixing zone characterized by high salinity (Robinson et al., 2006; Kroeger and Charette, 2008; Santos et al., 2009; Anwar et al., 2014). Between the SW and the USP, there is a confined freshwater discharge tube (FDT) that intersects the beach near the low tide (LT) mark. Around this FDT, geochemical conditions transit from a reduced, circumneutral pH freshwater to an oxygenated, higher pH seawater, which determines the chemical speciation and solubility of elements along the flow path.

Ferrous ions (i.e., Fe(II) or Fe^{2+}), as an element in groundwater owing to the abundance of iron-bearing minerals in Australia (Larrahondo and Burns, 2014), can undergo rapid oxidation to ferric ions (i.e., Fe(III) or Fe^{3+}) in the presence of dissolved oxygen (DO) in seawater (Viscarra Rossel et al., 2010). Compared to Fe(II), Fe(III) is less soluble and can precipitate as ferric oxyhydroxides (i.e., $Fe(OH)_3$) at the groundwater-seawater interface (Charette and Sholkovitz, 2002; Charette and Allen, 2006). Such precipitates in intertidal areas were observed by several field studies (Abal and Watkinson, 2000; Lloyd et al., 2009). Additional research indicated that the accumulation of these precipitates can act as a geochemical barrier retaining dissolved phosphate (PO_4^{3-}) within the coastal groundwater system (Charette and Sholkovitz, 2002; Spiteri et al., 2006; Lalonde et al., 2012; Linkhorst et al., 2017), thereby having a substantial impact on the regulation of subsurface chemical fluxes into the ocean. Thenceforth, the term “iron curtain” was proposed and has since gained widespread use to describe its environmental functionalities in coastal areas.

So far, SGD has been studied intensively with their response to continental processes (e.g., inland hydraulic heads) (Liu et al., 2016; Kuan et al., 2019; Mo et al., 2021) and oceanic oscillations (wave and tide particularly) (Li et al., 1999; Robinson et al., 2006; Xin et al., 2010; Shen et al., 2018). In contrast to the extensive numerical studies addressing coastal hydrogeological processes, limited research has been conducted on major ions and metals, and field-based studies on iron curtains are also scarce. However, major research efforts have been made to understand the geochemical zonation linked to iron (Fe) concentration and its speciation in the intertidal area (Gibbes et al., 2008; Roy et al., 2010; Porubsky et al., 2014; Reckhardt et al., 2015; Beck et al., 2016; Hanington et al., 2016; Paffrath et al., 2020). For instance, chemical analysis of porewater samples from an offshore site in North Stradbroke Island, Australia, revealed that dissolved Fe in groundwater primarily existed in the form of Fe(II); it also demonstrated the presence of high Fe(II) concentration compared to that in seawater (Gibbes et al., 2008). Furthermore, detailed measurements of Fe(II) concentrations obtained by incubating sediment cores from northern Deception Bay, Australia, provided evidence of Fe(II) efflux at the sediment-seawater interface (Hanington et al., 2016). Although these studies have delivered valuable insights into Fe in coastal areas, the understanding of subsurface processes remains incomplete because physical and geochemical processes are analyzed independently (Robinson et al., 2018). Henceforth, this results in a restricted comprehension of the spatial variations of the iron curtain and its impact on subsurface flow. In addition, the lack of field datasets poses challenges to the representativeness of model results. Therefore, there is still an urgent need for field data to improve the accuracy of numerical modeling.

In response to these research gaps, a field investigation was conducted at a sandy beach to explore both physical and geochemical processes in the intertidal area. This study aims to develop a conceptual model illustrating the transformation of Fe from an aqueous form to a solid phase in the coastal groundwater system. The research objectives are twofold: a) how geochemical conditions (e.g., pH and redox potential (Eh)) evolve from groundwater to seawater and influence the speciation and solubility of Fe in the intertidal area, and b) how Fe precipitates spatially vary along the groundwater-seawater interface to form a geochemical barrier that retains dissolved chemicals. This field-based study offered valuable datasets in assisting the comprehension of the geochemical transition from groundwater to seawater, and the conceptual model can help establish an effective procedure for accessing Fe transformation at the groundwater-seawater interface. In addition, this study contributes to an in-depth understanding of the evolution of coastal aquifers induced by these coupled processes and presents corresponding environmental functionalities in land-ocean connectivity through groundwater.

2 Field site

The field site (see Figure 1A) is a tidal beach with a mild slope ($\Delta h/\Delta L$ = 0.015) on the northern end of Deception Bay (27°5′3″S, 153°8′7″E, a part of Moreton Bay Region), Southeast Queensland, Australia. Moreton Bay is a sheltered coastal system protected by large sand islands (Moreton Island (Mulgumpin) and Stradbroke Island (Minjerribah)). The southern and western sides of Moreton Bay are strongly influenced by major river estuaries, which transport sediments into the bay, producing intertidal mudflats and mangrove swamps. The northern and eastern parts of the Bay have predominantly sandy beaches with occasional meadows. Based on the identification of probable freshwater features (rivers and creeks, but excluding rainfalls) in this region by incorporating field investigations with satellite maps, it is considered that the fresh groundwater is only from the northwest terrestrial environment (see Figure 1B).

This sandy beach was characterized by a subtidal and intertidal area that has been subjected to extensive and frequent Lygnbya blooms since the early 1990s (Albert et al., 2005). Up to the time of our field

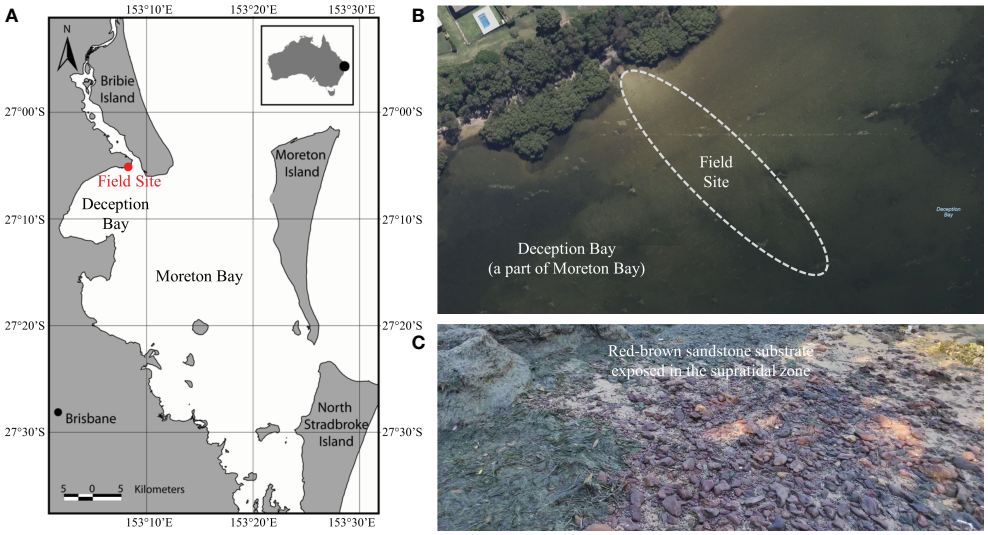

FIGURE 1
(A) Map of the field site in Sandstone Point, Southeast Queensland, Australia (adapted from Robinson et al., 2007). The field site is on the northern end of Deception Bay (27°5′3″S, 153°8′7″E), a part of the Moreton Bay Region protected by Moreton Island (Mulgumpin) and North Stradbroke Island (Minjerribah). **(B)** The sandy intertidal area of the field site with the nearby buildings and major vegetation; **(C)** Snapshot of red-brown sandstone substrate exposed in the supratidal zone of the field site, and the outcropping sediments were identified to contain Fe minerals in earlier studies.

investigation, more than 30 Lyngbya blooms had been observed by the ongoing *Lyngbya Monitoring Program* organized by the Queensland Government (Department of Environment, Science and Innovation, Queensland, Australia, 2013). The hypothesis that Lyngbya blooms can be exacerbated by the presence of Fe was proposed earlier (Hanington et al., 2016), and the outcropping sediments contain Fe minerals that were identified in earlier studies (Ahern et al., 2006a; Saeck et al., 2019). In addition, indurated Fe-rich sand crusts are exposed in proximity areas along the coastline (see Figure 1C), which supports the selection of this particular stretch of coast.

3 Field methodology

3.1 Monitoring system and equipment

The field investigation was conducted during spring tide in May 2021, and the field monitoring lasted five days from the 10th to the 14th of May 2021. It is widely accepted that the groundwater system, in this case, could be considered two-dimensional (2-D) under the Dupuit assumption for simplifying engineering-scale groundwater modeling (Liu et al., 2023). Additionally, it is assumed that there are minimal variations of the phreatic line (i.e., groundwater table) alongshore (Gibbes et al., 2007). Thus, a single cross-shore transect was selected from the landward of the high tide (HT) mark into the subtidal region in order to track groundwater processes in the intertidal area. Figure 2 shows a cross-shore transect that was 40 m in length and started from the HT mark. A field monitoring system was set up across the shoreline to take measurements, and all of the equipment was collectively placed in the intertidal area where there was a highly reactive area for porewater exchange. The exact position of the benchmark (BM) was identified using a GPS (Garmin Australasia Pty Ltd.), and the elevation was converted to the Australian Height Datum (AHD), which is the official vertical datum used in Australia. By following that, at the locations of equipment, their corresponding elevations in reference to the local BM were determined horizontally along this transect, using a self-leveling rotating laser (RL-H5A with a precision of ±1.5 mm, Topcon Positioning Systems Inc.).

Figure 2 illustrates the configuration of the monitoring system, which includes:

(1) The weather station, underpinned by a steel tripod, was electrically powered by a battery that was constantly recharged by a solar panel. It was also equipped with a remote-controlled datalogger, a weather-resistance camera, and a series of meteorological sensors, all of which were mounted on the tripod (see Figures 3A, B). Hence, the weather station could monitor the field conditions at a given interval, and the datalogger could record the datasets, which were subsequently sent to the internet-of-things (IoT) platform through a 3G/4G signal for instantaneous visualization

(2) The custom-made multi-level samplers (MLS, 2 m in length) were used to collect porewater samples to determine both physio-chemical variables and the chemical forms of dissolved Fe. As an improved design of those employed by Martin et al. (2003), each MLS comprises polyvinyl chloride (PVC) pipes (diameter of 50 mm, Holman Industries Pty Ltd.) with a threaded end and a pointed endcap, as well as ten sampling ports spaced at a spatial interval of 0.2 m along the pipe. They were installed at a 0.5 m offset to the piezometers at the site (see Figure 3A).

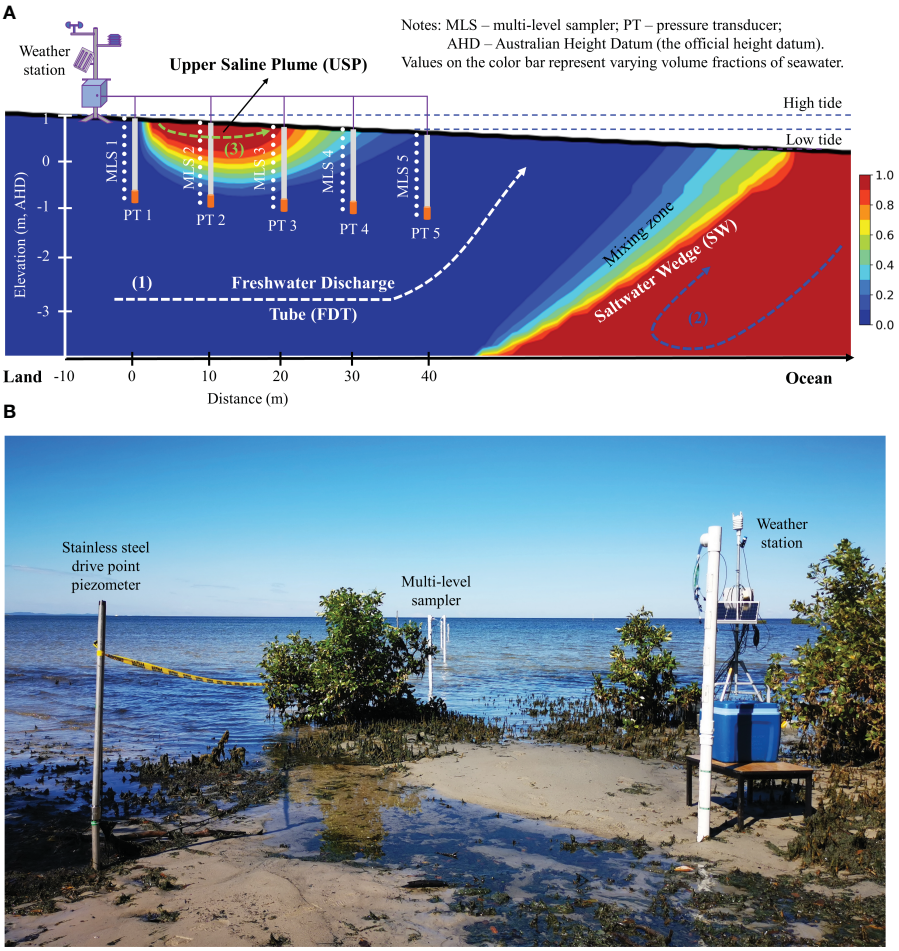

FIGURE 2
(A) Schematic diagram of field experimental setup in a coastal groundwater system. The bold black line is the beach profile. The horizontal direction represents the beach transect toward the ocean, and the vertical direction represents the elevation relative to the Australia Height Datum (AHD) which is the official height datum for Australia. As shown in the color bar, red indicates pure seawater with a volume fraction of 1.0, while blue represents pure fresh groundwater with a volume fraction of 0.0. In between the two is the mixing zone with varying volume fractions of seawater. The major processes in the intertidal area include (1) fresh groundwater discharge (shown as a white dashed line), (2) density-driven circulation (shown as a blue dashed line), and (3) tide-induced circulation (shown as a green dashed line). Between the saltwater wedge (SW) and the upper saline plume (USP), a freshwater discharge tube (FDT) intersects the beach. **(B)** Snapshot of field experimental setup along the beach transect in the intertidal area at Sandstone Point, Southeast Queensland, Australia. The field instruments included a solar-powered weather station, five multi-level samplers (MLS), and five drive point piezometers (equipped with pressure transducers (PT)) which were installed at 10-m intervals along the beach transect.

(3) An array of driving points of piezometers (equipped with PT, numbered PT1 to PT5 towards the ocean) was installed at 10 m intervals along this transect to record the temporal variations of the groundwater table driven by tidal fluctuations. As for borehole casing, several stainless steel standpipes (diameter of 25 mm, Solinst Inc.) were driven underground to the desired depth using a post driver. After casing those boreholes with stainless pipes, the bottom end of each pipe was covered by a screen within a length of 0.3 m. The sensors (AquaTROLL 200, In-Situ Inc.) in each borehole could instantaneously record the datasets of water level and pressure, electrical conductivity (EC), and temperature to the weather station at designated temporal intervals through a few data cables.

3.2 Field sampling and measurements

The porewater samples were collected using sampling ports at the MLS (see Figure 3A). As described in Figure 3B, the collected sample obtained from the spherical capture zone with a small radius (≈0.05 m) was representative of the porewater around the sampling port. The volume of each sample was limited to 120 mL to minimize the impact on the surrounding waters so that there was no cross-port interference and in-situ perturbation during porewater sampling. Figure 3C shows that porewater from each sampling port was extracted using a peristaltic pump (Geopump Series II, Geotech Environmental Equipment, Inc.) at a low flow rate of 60 mL/min and was rapidly transferred into a flow cell for a later determination of in-situ physio-chemical state variables (e.g.,

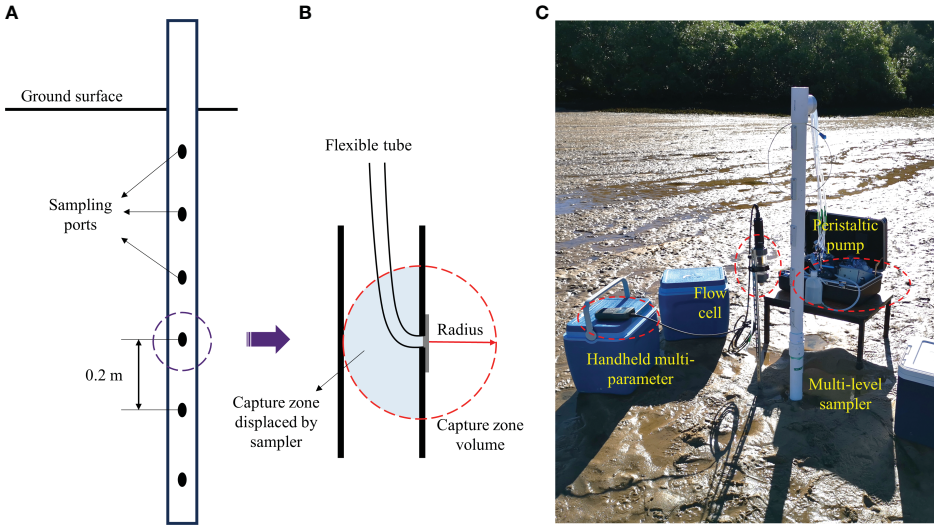

FIGURE 3
(A) Schematic diagram of MLS installed in the intertidal area. The sampling ports are spaced at a spatial interval of 0.2 m vertically. **(B)** Capture zone of each sampling port with a small radius of 0.05 m that limits the volume of porewater around the sampling port in order to prevent cross-port interference. **(C)** Snapshot of field sampling in the intertidal area. The porewater sampling procedure includes (1) extracting porewater with a peristaltic pump at a low flow rate; (2) transferring it into a flow cell for in-situ measurements using a handheld multi-parameter; (3) collecting the sample with a syringe and then transferring it into the sample bottle for storage.

salinity, DO, pH, and redox potential) using a portable probe (HI98194, Hanna Instruments, Inc.). The overflow collected by a syringe of 60 mL was thenceforth transferred into the high-density polyethylene (HDPE) plastic bottles through a sterile filter (filtering size = 0.45 μm). In order to stabilize the dissolved Fe in different chemical forms, the bottles were priorly acidified with hydrochloric acid (HCL), i.e., filling the container entirely. This step can effectively minimize any potential oxidation in storage during transport. Throughout the field investigation, porewater at each port was sampled twice per day, so it took 4–6 hours to reconstruct a complete profile by spatially interpolating the datasets collected from all ports. Although the spatial porewater measurements were not synchronized in terms of both equipment and operating procedure, all datasets were recorded within a single day, and this issue could be later resolved by temporal interpolation in the data post-analysis.

It was once suggested by Thamdrup et al. (1994) that porewater analysis is dependent on the collection of intact sediment cores where pore water samples are extracted, mainly when analysis of the solid phase is also undertaken (Gibbes et al., 2008). However, it was highly challenging to preserve the integrity of the sediment cores from the same location at different times. To provide an alternative resolution in this regard, additional sediments from ambient areas (within a diameter of 0.5 m) at each sampling location were manually retrieved underground using a hand auger in depths of 0.5 m and 1.0 m, respectively. Those sediments were directly transferred into glass containers to determine the content of Fe oxides. Moreover, when the intertidal area was exposed at low tides, the sediment core was collected by (1) pushing a plastic pipe (inner diameter 76 mm) vertically down into the sediment at the selected location; (2) carefully digging around the pipe with a spade or shovel to avoid excessive disturbance; (3) capping the pipe at the top to seal it completely at the maximum depth achievable; (4) slowly extracting the pipe from the sandy beach, and completely sealing the pipe at the bottom; (5) keeping it as upright as possible to minimize disturbance. As a result, three undisturbed sediment cores (two were Φ76 mm × L300 mm in burial depth, while one was Φ76 mm × L500 mm) were taken for additional analysis of the hydraulic and seepage properties.

3.3 Laboratory tests and analysis

The chemical analysis of those porewater samples was carried out in an environmental laboratory (ALS Ltd.). The concentration of total Fe in the sample was quantified using an inductively coupled plasma mass spectrometry (ICP-MS) (Agilent 7900, Agilent Technologies Pty Ltd.), while the specific concentration of Fe(II) was determined by a discrete analyzer which utilized ion selective electrodes (ISE) (Konelab Prime 60i, Thermo Fisher Scientific Inc.) The measured potential between each ISE and the reference electrode correlated with the natural logarithm of the ionic activity (as per the Nernst equation), which reflected changes across the ISE membrane/sample interface. Consequently, the concentration of Fe(III) was derived through a simple calculation employing the total Fe and dissolved Fe(II) values. Furthermore, the metals in sediments were extracted by an aqua regia digest (2 mL of 1:1 HNO_3 and 10 mL of 1:4 of HCl). The content of total Fe and total P was determined by an inductively coupled plasma -optic emission spectroscopy (ICP–OES) (Agilent 5110, Agilent Technologies Pty Ltd.) and a discrete analyzer (Konelab Prime 60i, Thermo Fisher Scientific Inc.), respectively.

Hydraulic conductivity (i.e., coefficient of permeability K in geomechanics) tests were conducted on sediment cores at the

Geomechanics Research Laboratory, School of Civil Engineering (SoCE) at the University of Queensland (UQ). The constant head method was utilized to measure the hydraulic conductivity by employing a Mariotte bottle to supply a constant hydraulic head at the boundary of the rigid-wall permeameter (ASTM D2434-68, 2006). In addition, the porosity of the in-situ sediment specimen was determined based on the theory of soil representative elementary volume (REV) in three-phase fractions (e.g., air, water, and solid); in order to achieve this, the specific gravity and dry density of in-situ specimen were measured separately using the gas pycnometer (ASTM D5550-23, 2023) and oven-drying methods (ASTM D7263-21, 2021). The particle size distribution (PSD) tests were performed on the sediment samples using the sieving method (ASTM D6913-17, 2021). The data obtained from porosity and effective particle size (d_{10}, d_{30}, and d_{60}), along with the Kozeny-Carman equation (see Equation 1), were used to estimate the hydraulic conductivity of the saturated sediment for comparison. It is crucial to repeat these tests at least three times and then take an average to eventually provide reliable hydraulic and seepage properties of the in-situ sediment specimens (Yan et al., 2022a, 2022b).

$$K = \frac{1}{C}\frac{\rho g}{\mu}\frac{n^3}{(1-n)^2}d^2 \quad (1)$$

where C is the shape factor (C = 180–270 for granular soil, such as sand), ρ is the water density (kg/m^3), g is the gravitational acceleration (m/s^2), μ is the water viscosity (Pa•s), n is porosity, d is the effective diameter (m), equivalent to the spatial mean diameter of pore hydraulic conduits (i.e., effective seepage flow paths).

4 Results and discussion

4.1 Tide-induced circulation and porewater exchange

Tidal data was collected from the gauge located at Scarborough Boat Harbour in northernmost Redcliffe, Queensland, Australia, which is approximately 10 km away from the studied site. The dataset covered a semi-diurnal tide from the 10th to the 14th of May 2021.

Figure 4 shows the field measurements in 2021 that occurred during spring tide. At HT, the water levels reached as high as 1.20 m, whereas they dropped to –0.80 m at LT. The observed condition in the field revealed that the investigated transect was inundated during HT while it became exposed to the atmosphere during LT. Consequently, the tidal force acting upon the beach led to notable porewater exchange processes in the intertidal area. Specifically, the receding tide resulted in porewater drainage from the intertidal area, which was later replaced by seawater infiltration during the rising tide. This semi-diurnal pattern can lead to the fluctuation of porewater physio-chemical variables in response to the groundwater table variations in the measured timeline. Tidal-induced circulation can contribute significantly to salt and solute transport in the intertidal area, which facilitates the exchange of geochemical conditions between the intertidal area and coastal seawater. This exchange mechanism plays an important role in the transformation and distribution of Fe in the porewater and sediment.

4.2 Porewater chemistry and oxidizing conditions

The porewater sampling was conducted during the daytime of 13th May 2021, aiming to study the geochemical conditions linked to Fe speciation in the beach transect, specifically focusing on the intertidal area. The manual measurements of extracted porewater samples were conducted twice at an interval of c.a. 4 h: (i) during HT when the intertidal area was inundated and (ii) during LT when it was exposed to the ambient atmospheric condition. Throughout the sampling, the temperature of extracted porewater was in the range of 20.1 °C to 22.6 °C, which suggested a minor impact on water density and viscosity, as well as on major physio-chemical variables, such as salinity, pH, DO, and Eh. Figure 5 illustrates the

FIGURE 4
Tidal readings at Scarborough Boat Harbour in northernmost Redcliffe, Queensland, Australia, located around 10 km away from the field site. The dataset captured semi-diurnal tide cycles (ranging from −0.8 m to 1.2 m based on the Australian Height Datum (AHD), the official vertical datum for Australia) between 10 May and 14 May 2021 (Source: Maritime Safety Queensland, Australia).

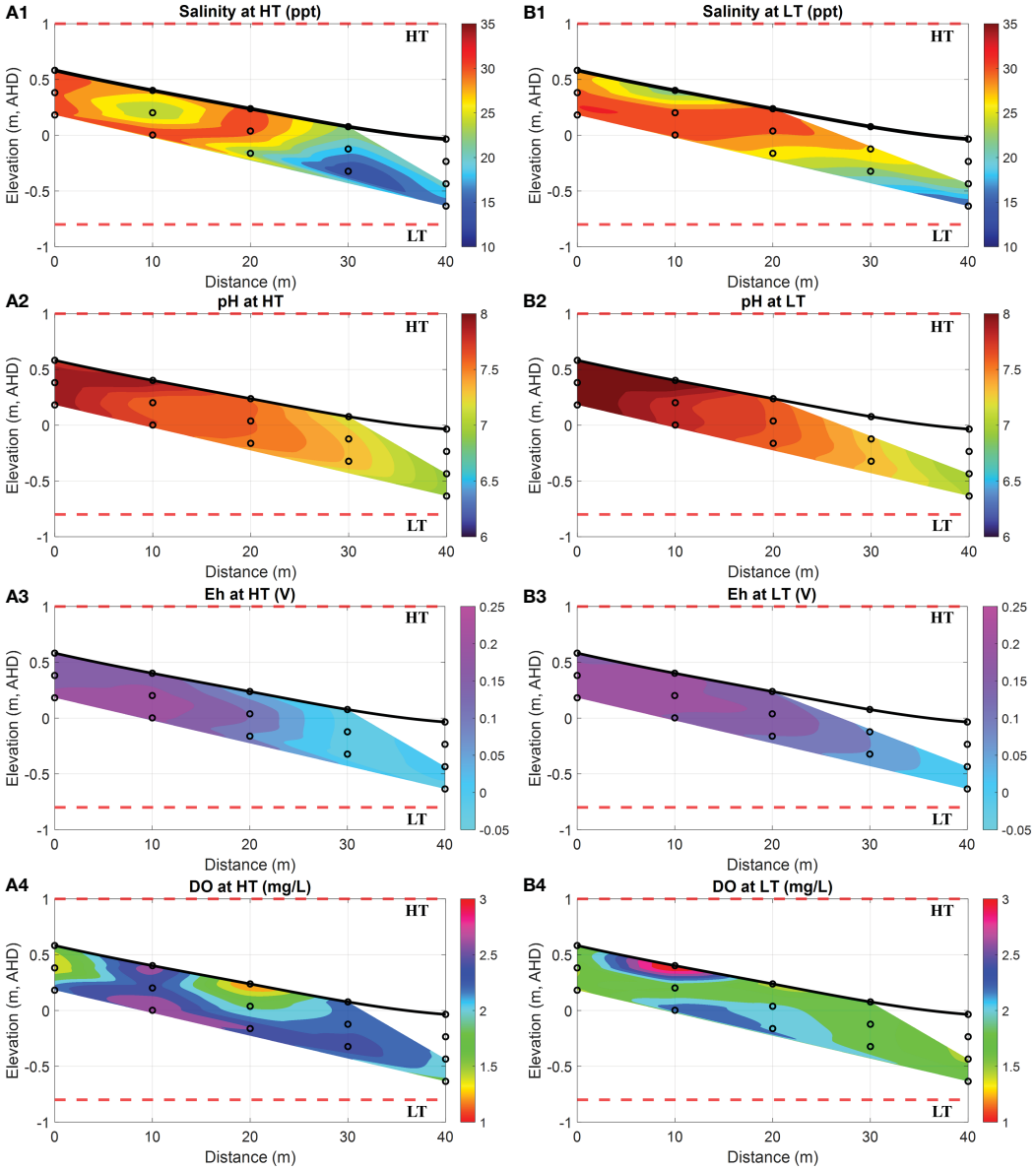

FIGURE 5
Spatial distribution of salinity, pH, Eh, and DO at HT and LT in the intertidal area. **(A1-A4)** show the salinity (in ppt, equivalent to g/kg), pH, Eh (in Volts) and DO (in mg/L) levels at HT, while **(B1-B4)** represent the salinity (in ppt, equivalent to g/kg), pH, Eh (in Volts) and DO (in mg/L) at LT. In addition, the bold black line is the beach profile, and the black circles represent the sampling points. The red dashed lines represent the HT and LT elevations in relation to the Australian Height Datum (AHD) which is the official vertical datum for Australia. The horizontal represents the distance towards the ocean, and the vertical represents the elevation relative to AHD.

spatial distribution of salinity, pH, Eh, and DO at HT and LT in the intertidal area. These data are essential for investigating major physio-geochemical mechanisms influencing the transformation of dissolved Fe(II) in the coastal groundwater system.

During both HT and LT, the porewater samples collected between the horizontal locations of 0 m and 20 m exhibited relatively high salinity, i.e., 31 ppt (a maximum value in orange areas of Figures 5A1, B1), along with a high pH value of 8.0 (a maximum value in dark red areas of Figures 5A2, B2). These findings suggested the presence of seawater in the submarine unconfined aquifer. Previous field observations also supported the existence of a USP due to tidal forces (Robinson et al., 2006, 2018). The tide-induced circulation maintained a surficial mixing zone with high salinity near the surface water infiltration area, consequently raising the pH value in the upper intertidal area. On the contrary, porewater samples collected from locations between 30 m and 40 m on the ocean side displayed relatively lower salinity at 15 ppt (a maximum value in blue areas of Figures 5A1, B1) and a moderate pH of 7.0 (a maximum value in green areas of Figures 5A2, B2), resembling the characteristics of fresh groundwater. Previous studies conducted near this site suggested that significant quantities of terrestrial fresh groundwater seep through soil profiles at depth and potentially are released into the offshore area of Deception Bay (Albert et al., 2005). Both the former

study and our field observations demonstrated that terrestrial groundwater was being transported to the adjacent intertidal area in the specific section of the transect along the beach.

Furthermore, DO measurements (see purple areas in Figures 5A4, B4) revealed a stripping zone with a high concentration of oxygen that reached up to 3.1 mg/L. This DO-rich seawater infiltrated into the intertidal transect due to tidal forcing. Consequently, a significant amount of DO entered the surface water infiltration zone, and thereby, it led to the high content of DO extending into the USP. However, the DO in this zone could be rapidly depleted through oxidation processes. As a result, the extent of the area with a relatively high content of DO exhibited dynamic variations over tidal cycles, which were attributed to the residence time of seawater circulation during the spring-neap tide (Robinson et al., 2007). Moreover, Eh is a parameter used to describe the tendency of a chemical species to either undergo reduction by accepting electrons or oxidation by donating electrons (Reddy, 2000). Its value of >0.1 V indicates oxic environments (Scholz, 2019). As shown in Figures 5A3, B3, the high values of Eh ranging from 0.1 V to 0.25 V between the horizontal locations of 0 m and 20 m indicated a strong oxidizing environment for redox-sensitive Fe(II), consistent with the pattern observed for DO (see purple areas in Figures 5A4, B4). Specifically, the oxidizing conditions were prominent at the seawater infiltration point from 0 m to 20 m, where a higher content of DO was observed. Meanwhile, the receding Eh (see cyan areas in Figures 5A3, B3) was observed at the groundwater discharging point between the horizontal locations of 30 m and 40 m.

More importantly, in contrast to the high concentrations of DO (see Figure 6A4) observed at high tides, Figure 6B4 demonstrated an exceptionally high DO concentration in porewater near the sediment surface. This phenomenon may be attributed to a combination of factors, including the short residence time of USP and air intrusion during desaturation periods. Considering the porewater sampling duration of 4–6 hours, air intrusion could become available at low tides when the intertidal area was exposed to the ambient environment. This exposure allowed air to infiltrate into the sediment, particularly into the surface layers where pore spaces were more accessible. As air infiltrated, oxygen from the atmosphere slowly dissolved into the porewater, which resulted in elevated levels of DO near the sediment–atmosphere interface. However, a high salinity observed between the distances of 5~15 m (see Figure 5A1) indicated the possible residence of USP and tidal influences on oxygen penetration, which may also contribute to the high DO levels observed in deeper sediment layers at the same location, as illustrated in Figure 5B4.

4.3 Fe transformation and phosphate removal

Further chemical analysis on porewater samples was carried out in the laboratory to determine the concentrations of dissolved Fe(II) and Fe(III) as well as PO_4^{3-}. As a result, Figure 6 illustrates the distribution of Fe(II), Fe(III) and PO_4^{3-} at HT and LT on 13th May 2021. In contrast to the low concentrations of PO_4^{3-}, the results at

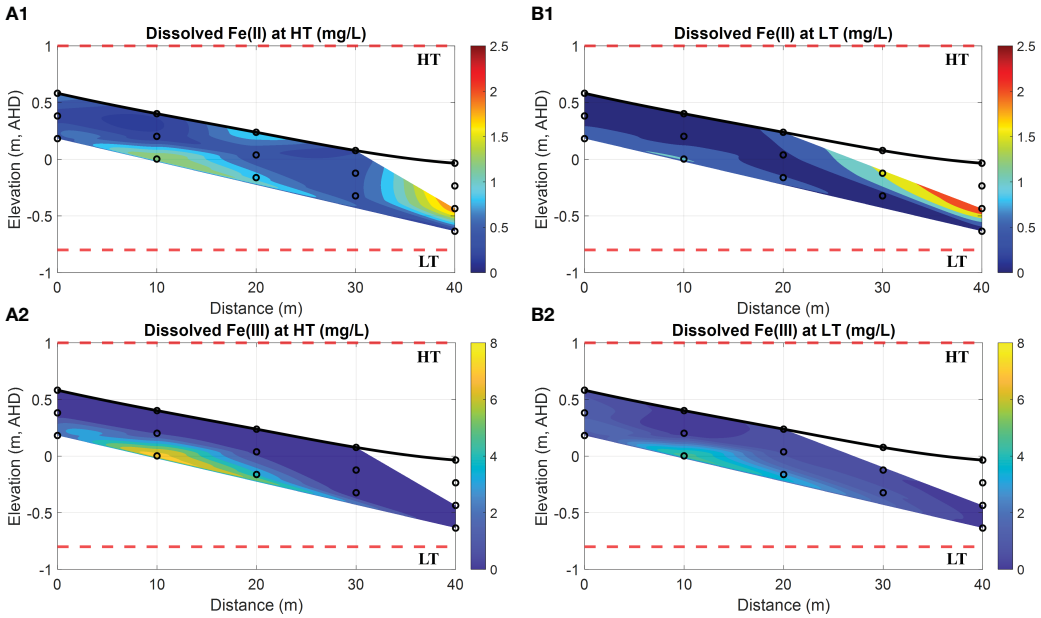

FIGURE 6
Spatial distribution of dissolved Fe(II) and Fe(III) at HT and LT in the intertidal area. **(A1,A2)** show the dissolved Fe(II) and Fe(III) (both in mg/L) at HT, respectively, while **(B1, B2)** represent the dissolved Fe(II) and Fe(III) (both in mg/L) at LT, respectively. In addition, the bold black line is the beach profile, and the black circles represent the sampling points. The red dashed lines represent the HT and LT elevations in relation to the Australian Height Datum (AHD) which is the official vertical datum for Australia. The horizontal represents the distance towards the ocean, and the vertical represents the elevation relative to AHD.

both HT and LT indicate that the porewater contains a substantial amount of Fe(II) in a range of 0.08~2.52 mg/L. However, a significant concentration of Fe(II) peaking at 1.99 mg/L or 2.52 mg/L was only observed in a restricted region at a distance of 40 m (see red area in Figures 6A1, B1).

Based on the chemical analysis of porewater samples taken between the horizontal locations of 0 m and 20 m, there was a presence of relatively low Fe(II) concentrations (with a maximum value of 1.01 mg/L, see cyan areas in Figures 6A1, B1) in the upper intertidal area, while high concentrations of dissolved Fe(III) (>5.0 mg/L, see yellow areas in Figures 6A2, B2) were observed in the same region. Upon comparing these patterns with the DO concentrations in Figures 5A4, B4, it is evident that the majority of Fe(II) had been oxidized to Fe(III) due to the strong oxidization at the bottom interface of the USP. In contrast, at the horizontal locations between 30 m and 40 m, relatively high concentrations of dissolved Fe(II) (within 0.8~1.8 mg/L, see red areas in Figures 6A1, B1) coincided with the environment characterized by lower values of DO and Eh at the exit of fresh SGD. Our field investigation, combined with previous studies on other sites near the current (Hanington et al., 2016), further supported the notion of benthic Fe released into Deception Bay through SGD. Moreover, by comparing Figures 6A2, B2, it was observed that the oxidation process from Fe (II) to Fe(III) during HT could be more significant than during LT. The reason is that tidal circulation provided more DO to the USP, which thereby facilitated the Fe(II) oxidation at the groundwater-seawater interface.

Furthermore, high concentrations of Fe(III) (up to 4.6 mg/L in a specific location) observed in porewater may contradict the conventional understanding of its limited solubility in aquatic environments. The discrepancy can be explained by the possible biogeochemical processes that are prevalent in anaerobic environments such as marine sediments and groundwater systems (Spiteri et al., 2008; McAllister et al., 2015; Sukekava et al., 2024). Due to possible microbial activities in aquatic settings, precipitated Fe oxides could undergo dissolution and re-precipitation, which allows them to alternate between ferrous and ferric states. Specifically, Fe-reducing bacteria can reduce Fe(III) within Fe oxides to more mobile and soluble Fe(II), while Fe-oxidizing bacteria transform Fe(II) into insoluble Fe(III) which then precipitates as solid-phase Fe oxides (Luef et al., 2013; Kügler et al., 2019; Baker et al., 2023). Consequently, such biogeochemical processes can profoundly influence the stability and remobilization of Fe oxides, which in turn influence the concentration and distribution of dissolved Fe(II) and Fe(III) in natural field conditions. Although Fe remobilization is beyond the scope of this study, the field investigation holds promise for further advancements in subsequent studies.

Figure 7 exhibits a consistently low concentration of dissolved PO_4^{3-} in porewater. Nevertheless, the PO_4^{3-} concentration observed between the horizontal locations of 0 m and 30 m (see cyan areas in Figures 7A, B) was less significant than that from 30 m to 40 m (see magenta areas in Figures 7A, B), referred to as the exit of fresh SGD (see blue areas in Figures 5A1, B1). This discrepancy implies a substantial decrease in phosphate concentration as the fresh groundwater moves through the FDT, as illustrated in Figure 2A, attributed to the presence of Fe oxides in the sediment. The subsequent analysis of sediment can provide evidence that Fe oxides can serve as a sink for dissolved PO_4^{3-} in this intertidal area.

4.4 Sediment chemistry and spatial heterogeneities

Based on the laboratory tests conducted at UQ, the physical properties, including seepage and hydraulic properties, of coastal sediment specimens are presented in Table 1. The results indicate that the sediment specimens can be classified as SP, which stands for poor-graded quartz sand, based on the unified soil classification system (USCS). Besides, these specimens contained a fine content (<0.075 mm) of 0.1%, according to the PSD test.

In addition, Figure 8 shows a 2-D cross-sectional beach transect that illustrates the spatial distribution of Fe oxides and phosphorous-containing compounds within the sediment.

Figure 8A shows three distinct regions (named Region #1, #2, and #3 in order) with intensive Fe that can be identified. Specifically, Region #1 was located at 0 m, closer to the ground in the upper

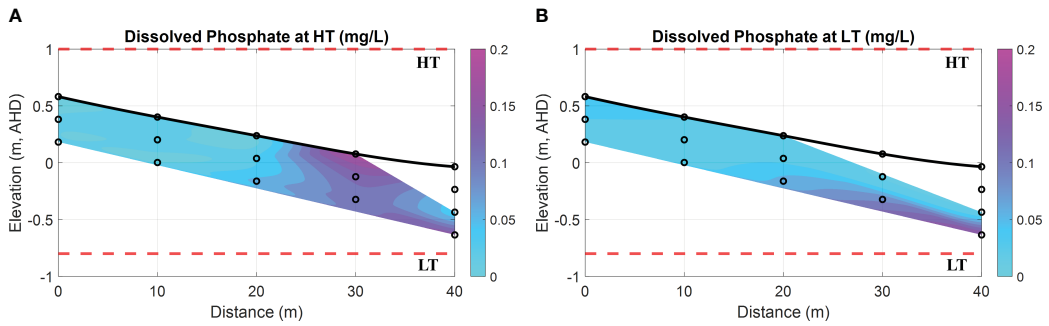

FIGURE 7
Spatial distribution of dissolved phosphate (PO_4^{3-}) at HT and LT in the intertidal area. **(A)** dissolved PO_4^{3-} (in mg/L) at HT; **(B)** dissolved PO_4^{3-} (in mg/L) at LT. In addition, the bold black line is the beach profile, and the black circles represent the sampling points. The red dashed lines represent the HT and LT elevations in relation to the Australian Height Datum (AHD) which is the official vertical datum for Australia. The horizontal represents the distance towards the ocean, and the vertical represents the elevation relative to AHD.

TABLE 1 Specification of coastal sediment specimens.

Category	Description	Value
Quartz sand	Dry density, $\rho_{d,max}$ (g/cm^3)	1.63
	Dry density, $\rho_{d,min}$ (g/cm^3)	1.59
	Porosity responding to dry density, n (-)	0.33~0.35
	Effective particle size, d_{10} (mm)	0.21
	Effective particle size, d_{30} (mm)	0.31
	Effective particle size, d_{60} (mm)	0.42
	Coefficient of uniformity, C_u	2.00
	Coefficient of curvature, C_c	1.09
	Estimated coefficient of permeability, K ($\times 10^{-4}$ m/s)	1.81~2.29 [a]

[a] Some values in this range were estimated by the Kozeny-Carman equation (see Equation 1).

intertidal area, whereas Region #2 was at 10 m with a depth of 1 m beneath the surface. Both regions exhibited substantial Fe, reaching up to 5220 mg/kg and 5830 mg/kg, respectively. Furthermore, Region #3 was suited at 40 m towards the ocean, and the total Fe peaked at 6520 mg/kg. Consequently, the spatial distribution of Fe along these regions displayed a strip-like pattern extending from the land to the ocean, corresponding to the bottom interface of the USP as shown in Figures 6A1, B1. This phenomenon can be attributed to the precipitation of Fe at the groundwater-seawater interface, a consequence of the subsurface mixing of Fe(II)-rich groundwater and DO-rich seawater. Through this mechanism, precipitated Fe can accumulate over time in the intertidal area, and this particular zone is commonly referred to as the iron curtain. It is important to acknowledge that the formation of an iron curtain is considerably more complex in the natural coastal environment and requires tens of thousands of years due to slow reaction kinetics. For example, the oxidative precipitation of Fe(II) exhibits a rate constant of 6.4×10^{-2} mmol^{-1}s^{-1} (Anwar et al., 2014).

Although several aspects, such as the aging process (Houben, 2003) and reduction process by microbial activities (Sevinç Şengör et al., 2007), were beyond the scope and capacities within the time scale of this investigation, the notable discrepancy in the concentrations of dissolved Fe(II) (up to 2.52 mg/L) and Fe(III) (up to 4.6 mg/L) was observed in local porewater samples when compared to their nanomolar levels conventionally found in aquatic settings. Such difference could be induced by possible biogeochemical processes, particularly when highly reactive Fe oxides were present in marine sediments. Previous studies have demonstrated that biogeochemical processes are prevalent in anaerobic environments (Spiteri et al., 2008; McAllister et al., 2015). In addition to pH-Eh conditions, two significant scenarios can influence the transformation, mobilization, and distribution of Fe speciation in groundwater systems. First, microorganisms play an important role in mediating Fe speciation through biological processes (Alotaibi et al., 2015; Wu et al., 2019). Microbial oxidation reactions, facilitated by Fe-oxidizing bacteria, transform Fe(II) to Fe (III) and promote the precipitation of Fe oxides in aerobic settings, whereas microbial reduction processes, driven by Fe-reducing bacteria, convert Fe(III) to Fe(II) and facilitate the remobilization of Fe oxides under anaerobic conditions (Luef et al., 2013; Baker et al., 2023). Second, Fe ions can form complexes with various ligands, including organic matter, humic substances, and inorganic ligands, which alter the solubility, stability, and reactivity of Fe speciation (Zhou et al., 2015; Sukekava et al., 2024). For example, organic ligands can enhance the solubility of Fe(III) by forming soluble Fe-organic complexes (Kügler et al., 2019). As a result, the combined effects of these factors determine the mobility and availability of Fe speciation in porewater and sediments within natural field settings.

With a specific surface area ranging from 530 m^2/g to 710 m^2/g (Hiemstra et al., 2019), ferrihydrite has a high capacity for adsorbing dissolved PO_4^{3-}. This characteristic results in the co-precipitation of Fe oxides and phosphorous-containing compounds (Chambers and Odum, 1990; Cornell and Schwertmann, 2003; Van Der Grift et al., 2016). Hence, the formation of Fe oxides can be regarded as a mechanism for sinking dissolved PO_4^{3-} in sandy sediment. In Figure 8B, high P content was observed in the intertidal sediment,

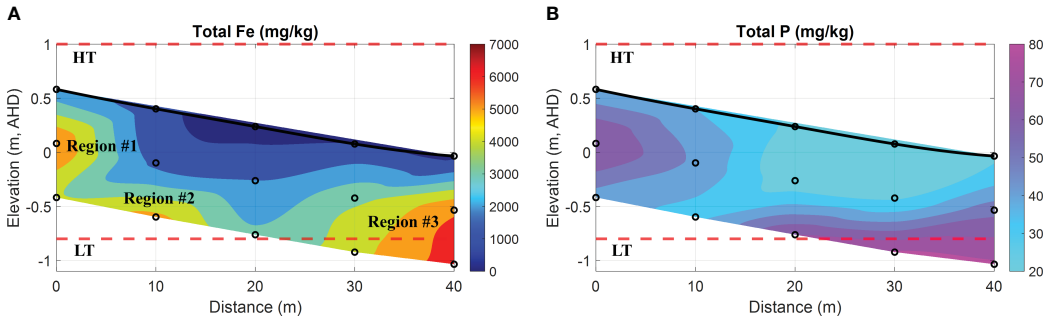

FIGURE 8
Spatial distribution of total Fe and P in the intertidal sediments. **(A)** total Fe oxides (represented as Fe in mg/kg); **(B)** total phosphorous-containing compounds (represented as P in mg/kg). In addition, the bold black line is the beach profile, and the black circles represent the sampling points. The red dashed lines represent the HT and LT elevations in relation to the Australian Height Datum (AHD) which is the official vertical datum for Australia. The horizontal represents the distance along the transect, and the vertical represents the elevation relative to AHD.

and the spatial distribution of total P in the field was consistent with that of total Fe in comparison with Figure 8A. The finding provides additional evidence to support the linear correlation between Fe oxides and P contents in the coastal bay, as investigated by (Charette and Sholkovitz, 2002; Testa et al., 2002). Furthermore, the analysis of seepage properties (e.g., hydraulic conductivity *K*) at various depths revealed that the *K* value at 1 m depth was averaged at 9.64×10^{-6} m/s, whereas the surface sediment had an estimated value of $(1.81\sim2.29) \times 10^{-4}$ m/s (see Table 1). The disparity between both was apparent, with a magnitude difference of up to two orders. According to the studies by (Carter and Bentley, 1991), the range of *K* values for poorly graded sands with little fines is typically between 5.35×10^{-5} m/s to 2.55×10^{-4} m/s. Therefore, the variation of *K* observed in the coastal sediment collected from two different depths can be attributed to the process of Fe precipitation or co-precipitation, rather than natural consolidation of beach sands. It is anticipated that this process will indefinitely continue unless a self-limiting mechanism is taken into account, such as the complete clogging of pore space. This would lead to the obstruction of porewater exchange, consequently influencing the evolution of the coastal groundwater system. However, it is beyond the scope of this investigation due to the time scale.

4.5 Sources of Fe and mobilization of Subterranean Fe

While Fe is the fourth most abundant element in the earth's crust (LePan and Venditti, 2021), the concentration of dissolved Fe (II) is typically very low (nanomolar-to-subnanomolar range) due to rapid oxidation to Fe(III) in oxygenated seawater with a pH > 7.0 (Fitzsimmons and Conway, 2023). Consequently, Fe(III) is more predominant than Fe(II), albeit still relatively low in concentration due to its low solubility in water bodies (Zhang et al., 2022). As shown in Figure 6A1, the transient peak of Fe(II) concentration at the groundwater-seawater interface reached 2.52 mg/L, which was eleven times higher than the value of 0.23 mg/L (data on 27 August 2018) observed in the borehole groundwater at a depth of 19.8 m in South Bribie Island, Queensland, Australia. Thus, the elevated concentration of Fe(II) in porewater is likely derived from a dissolved form of Fe(II) linked to local groundwater systems.

According to earlier studies, Sandstone Point is situated on a coastal plain with the underlying Landsborough Sandstone, characterized by quartz sand and consisting of Fe-rich minerals (Cox and Preda, 2005; Ahern et al., 2006b). Moreover, the intertidal area off Sandstone Point was subject to sampling in 2000. The report indicated that the soil was acidic (pH = 4.6~5.2) below a depth of 0.2 m and strongly acidic (pH< 3.4) at depths of 1~1.2 m (Albert et al., 2005; Ahern et al., 2006a). These findings suggest the presence of acid sulfate soils (ASS), which are omnipresent in the coastal areas of Queensland. When these soils are hydromechanically perturbated (e.g., agriculture and construction), the sulfides are exposed to air and react with oxygen to form sulfuric acid. This process leads to the decomposition of iron-bearing minerals (Manson et al., 2003), subsequently resulting in the release of iron ions into groundwater systems through rainwater infiltration and drainage systems (Larrahondo and Burns, 2014). As a result, surface soil samples (at depths of 0.2~0.3 m) exhibited low-to-moderate content of extractable Fe (up to 91 mg/kg), and elevated concentration of dissolved Fe(II) was identified in the groundwater, reaching up to 1.6 mg/L. This implies that significant volumes of fresh groundwater transport through the soil profiles at depth, transporting chemical solutes (including dissolved Fe(II)) to the adjacent intertidal area in Deception Bay, Queensland, Australia (Albert et al., 2005). The benthic release of Fe(II) was further validated through additional field and laboratory studies (Ahern et al., 2006a; Hanington et al., 2016; O'Neil and Dennison, 2016). Additionally, as emphasized in Section 4.4, biogeochemical mechanisms, particularly microbial reduction processes driven by Fe-reducing bacteria, may potentially convert Fe(III) to Fe(II) under anaerobic conditions, thereby facilitating the remobilization of Fe oxides in marine sediments. Its coupling with changes in pH and redox (i.e., Eh) conditions may ultimately determine the spatial distribution and concentration of Fe (II) in its dissolved form. This straightforward analysis indicates that a relatively high concentration of dissolved Fe(II) (see Figure 6A1) can likely be observed in porewater at the site under appropriate redox conditions.

In terms of geochemistry, the mixing of fresh groundwater and circulated seawater dominates the geochemical conditions along the flow path (see Figure 9). So biogeochemical zonations are created, and these zonations significantly affect the transformation, mobility, and removal of chemicals through the FDT. With respect to this field investigation, the mixing of Fe(II)-rich groundwater with oxygenated seawater in the intertidal area has been observed to induce the precipitation of Fe oxides at the groundwater-seawater interface beneath the USP. The accumulation of these minerals forms a less well-defined geochemical barrier, commonly referred to as an iron curtain, which has the capacity to retain dissolved chemicals such as phosphate. While this process can be viewed as a self-regulation mechanism affecting the ecology of coastal waters, specifically the nitrogen to phosphorus ratios (i.e., N/P), the discharge of freshwater with elevated Fe(II) could transport a substantial amount of bio-available Fe, which has the potential to stimulate the growth of Lyngbya. This influx of Fe(II) via SGD may represent a factor that has not received sufficient attention but contributes to the occurrence of Lyngbya blooms in the nearshore. To better address this concern, a more comprehensive field setup and an extended period of groundwater monitoring are required, and they need to incorporate reaction kinetics and site-specific information on major dissolved and solid-phase Fe, as well as the growth of Lyngbya.

5 Summary and prospects

The previous studies on the intertidal area primarily focused on groundwater flow and salt transport in an unconfined aquifer, with little emphasis on the transformation of redox-sensitive Fe(II) and the coupling between physical process (e.g., tide) and geochemical process (e.g., oxidative precipitation) along the seepage flow path.

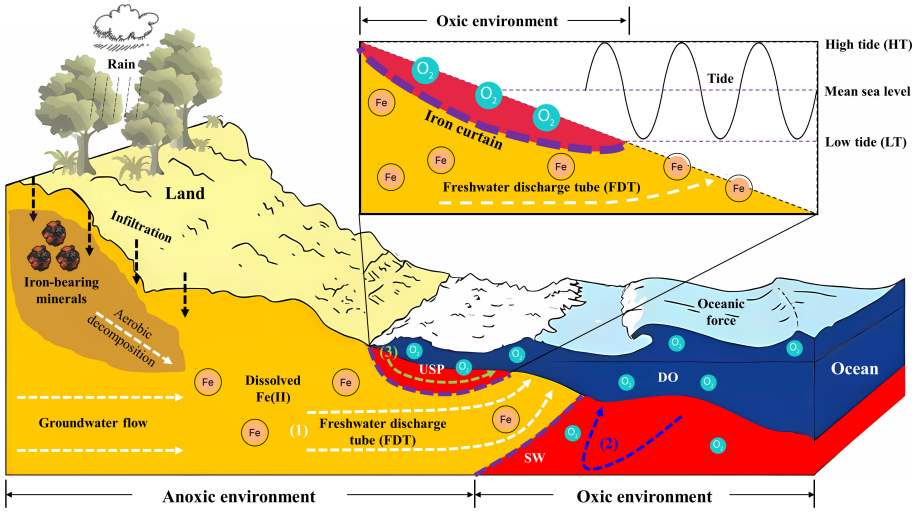

FIGURE 9
Conceptual model illustrating the hydrological and geochemical processes in the intertidal area. The delineated areas indicate distinct zones in the coastal environment: the orange area signifies the aquifer zone dominated by fresh groundwater, while the red area shows the seawater intrusion driven by oceanic oscillations such as tides. Within the intertidal area, three major processes include (1) fresh groundwater discharge (depicted by a white dashed line), (2) density-driven circulation (illustrated by a blue dashed line), and (3) tide-induced circulation (represented by a green dashed line). Between the saltwater wedge (SW) and the upper saline plume (USP), a freshwater discharge tube (FDT) intersects the beach. Moreover, the decomposition and dissolution of Fe-bearing minerals can lead to the release of Fe ions into groundwater systems (e.g., facilitated by rainwater infiltration as seen in a black dashed line). Fe(II)-rich groundwater can be oxidized by DO-rich seawater, and precipitate Fe oxides at the groundwater-seawater interface. The accumulation of these minerals can generate the iron curtain which acts as a geochemical barrier (shown by purple dashed lines) in the coastal aquifer system.

This study investigated the dynamics of porewater exchange and Fe speciation by conducting groundwater monitoring and sampling in a coastal bay. The field datasets provided concrete evidence of the subsurface mixing between fresh groundwater and oxygenated seawater, as well as the Fe transformation from an aqueous form to a solid phase at the groundwater-seawater interface beneath the USP. The findings also demonstrated the occurrence of an iron curtain that was observed to adsorb dissolved phosphate within the mixing zone of USP. Based on these field outcomes and corresponding implications, the research contributions can be summarized as follows:

A comprehensive field investigation demonstrated a geochemical transition from groundwater to seawater in the intertidal area. This area was characterized by the tide-induced circulating seawater and the discharge of fresh groundwater beneath. The dynamic process of groundwater-seawater mixing created a USP, a highly reactive zone that determined the speciation and solubility of Fe transporting through the FDT. Consequently, a substantial increase in DO concentration was observed, which created a localized hotspot with increased Eh. This indicated an oxidizing environment for Fe(II)-rich groundwater beneath and led to the oxidative precipitation of Fe(II) at the groundwater-seawater interface. Therefore, the sediment analysis revealed a spatial distribution of precipitated Fe with a strip-like pattern along this interface from land to the ocean. These regions with intensive accumulation of Fe oxides can be referred to as the iron curtain, acting as a geochemical barrier to retain dissolved phosphate by changing the seepage properties of coastal sediment. The field results indicated that the characterization of pH, DO, Eh and PO_4^{3-} profiles can be utilized as a practical approach to investigating and positioning the presence of iron curtains in the coastal area.

Furthermore, upon the geological settings and earlier studies conducted at Sandstone Point, Queensland, Australia, a conceptual model was developed to illustrate the origin of dissolved Fe and its mobilization associated with groundwater flow in the intertidal area. As described in Figure 9, the aerobic decomposition of iron-bearing minerals resulted in the release of iron ions into groundwater systems through infiltration. Subsequently, significant volumes of fresh groundwater delivered these dissolved ions to the adjacent intertidal area of the coastal bay. This process resulted in a notable concentration of dissolved Fe(II), and a peak value of 2.5 mg/L was observed in porewater at our site (see red areas Figures 6A1, B1), which was several orders of magnitude higher than that in seawater. In addition, the benthic release of additional Fe(II) could have the potential to stimulate the growth of Lyngbya in water bodies, and it is a factor that has received insufficient attention but contributes to the occurrence of Lyngbya blooms in the nearshore of Deception Bay, Queensland, Australia. Further investigations are still needed to better address the link between Fe and Lyngbya.

In summary, this study presents significant advancements in refining a conceptual model that explores the mobilization and transformation of Fe associated with coupled physical and geochemical processes due to groundwater-seawater mixing. Comprehending these processes provides valuable insights into the effect of tide-induced circulation on the speciation of redox-sensitive chemicals and the evolution of coastal aquifers. Although Fe minerals and microbial activities are very complex, introducing some uncertainties into flow and transport processes that were not

included in this research, the field outcomes establish a useful database and a unique opportunity to unravel the mechanism driving the formation of iron curtains and their environmental functionalities. In the long term, further investigations based on this study will contribute to more accurate predictions of future conditions, leveraging current seepage and geochemical features. This, in turn, will facilitate the development of improved strategies for sustainable management of coastal and marine ecosystems.

Data availability statement

The original contributions presented in the study are included in the article/Supplementary Material. Further inquiries can be directed to the corresponding authors.

Author contributions

WC: Conceptualization, Data curation, Formal analysis, Investigation, Methodology, Visualization, Writing – original draft, Writing – review & editing. HH: Methodology, Project administration, Resources, Supervision, Writing – review & editing. GY: Writing – review & editing. AS: Project administration, Supervision, Writing – review & editing.

Funding

The author(s) declare that financial support was received for the research, authorship, and/or publication of this article. This study was funded by the Australian Research Council through its Discovery Project (grant number: DP190103782).

Acknowledgments

The field monitoring design benefited from the original ideas of Professor Ling Li at Westlake University, and the collection of field data was assisted by Dr Chenming Zhang and Mr Zicheng Zhao at the University of Queensland. The authors thank the Queensland Government, the School of Civil Engineering and the School of the Environment at the University of Queensland for their support, and also appreciate the reviewers and editor for constructive comments on this paper.

Conflict of interest

The authors declare that the research was conducted in the absence of any commercial or financial relationships that could be construed as a potential conflict of interest.

Publisher's note

Supplementary material

The Supplementary Material for this article can be found online at: https://www.frontiersin.org/articles/10.3389/fmars.2024.1385517/full#supplementary-material

References

Abal, E., and Watkinson, A. (2000). *Investigation of Causes and Management of Lyngbya Blooms in SEQ*. PASSCON 2000 Pumicestone Passage and Deception Bay Catchment Conference, Brisbane, QLD Australia.

Ahern, K. S., O'Neil, J. M., Udy, J. W., and Albert, S. (2006a). Effects of iron additions on filament growth and productivity of the cyanobacterium Lyngbya majuscula. *Mar. Freshw. Res.* 57, 167. doi: 10.1071/MF05022

Ahern, K. S., Udy, J. W., and Pointon, S. M. (2006b). Investigating the potential for groundwater from different vegetation, soil and landuses to stimulate blooms of the cyanobacterium, Lyngbya majuscula, in coastal waters. *Mar. Freshw. Res.* 57, 177. doi: 10.1071/MF05115

Albert, S., O'Neil, J. M., Udy, J. W., Ahern, K. S., O'Sullivan, C. M., and Dennison, W. C. (2005). Blooms of the cyanobacterium Lyngbya majuscula in coastal Queensland, Australia: disparate sites, common factors. *Mar. pollut. Bull.* 51, 428–437. doi: 10.1016/j.marpolbul.2004.10.016

Alotaibi, M. D., Patterson, B. M., McKinley, A. J., Reeder, A. Y., Furness, A. J., and Donn, M. J. (2015). Fate of benzotriazole and 5-methylbenzotriazole in recycled water recharged into an anaerobic aquifer: Column studies. *Water Res.* 70, 184–195. doi: 10.1016/j.watres.2014.11.040

Anwar, N., Robinson, C., and Barry, D. A. (2014). Influence of tides and waves on the fate of nutrients in a nearshore aquifer: Numerical simulations. *Adv. Water Resour.* 73, 203–213. doi: 10.1016/j.advwatres.2014.08.015

ASTM D2434-68 (2006). *Test Method for Permeability of Granular Soils (Constant Head)*. ASTM International, West Conshohocken, PA, USA. doi: 10.1520/D2434-68R06

ASTM D5550-23 (2023). *Test Method for Specific Gravity of Soil Solids by Gas Pycnometer*. ASTM International, West Conshohocken, PA, USA. doi: 10.1520/D5550-23

ASTM D6913-17 (2021). *Test Methods for Particle-Size Distribution (Gradation) of Soils Using Sieve Analysis*. ASTM International, West Conshohocken, PA, USA. doi: 10.1520/D6913_D6913M-17

ASTM D7263-21 (2021). Test methods for laboratory determination of density (Unit weight) of soil specimens. *ASTM Int.* ASTM International, West Conshohocken, PA, USA. doi: 10.1520/D7263-21

Baker, I. R., Matzen, S. L., Schuler, C. J., Toner, B. M., and Girguis, P. R. (2023). Aerobic iron-oxidizing bacteria secrete metabolites that markedly impede abiotic iron oxidation. *PNAS Nexus* 2, pgad421. doi: 10.1093/pnasnexus/pgad421

Beck, A. J., Kellum, A. A., Luek, J. L., and Cochran, M. A. (2016). Chemical flux associated with spatially and temporally variable submarine groundwater discharge, and chemical modification in the subterranean estuary at gloucester point, VA (USA). *Estuaries Coasts* 39, 1–12. doi: 10.1007/s12237-015-9972-0

Carter, M., and Bentley, S. P. (1991). *Correlations of Soil Properties* (London: Pentech Press Publishers).

Chambers, R. M., and Odum, W. E. (1990). Porewater oxidation, dissolved phosphate and the iron curtain: Iron-phosphorus relations in tidal freshwater marshes. *Biogeochemistry* 10, 37–52. doi: 10.1007/BF00000891

Charette, M. A., and Allen, M. C. (2006). Precision ground water sampling in coastal aquifers using a direct-push, shielded-screen well-point system. *Groundwater Monit. Remediation* 26, 87–93. doi: 10.1111/j.1745-6592.2006.00076.x

Charette, M. A., and Sholkovitz, E. R. (2002). Oxidative precipitation of groundwater-derived ferrous iron in the subterranean estuary of a coastal bay. *Geophys. Res. Lett.* 29, 85-1-85–4. doi: 10.1029/2001GL014512

Cornell, R., and Schwertmann, U. (2003) *The Iron Oxides: Structure, Properties, Reactions, Occurrences and Uses*. Weinheim, Germany: Wiley-VCH Verlag GmbH & Co. KGaA. doi: 10.1002/3527602097

Cox, M. E., and Preda, M. (2005). Trace metal distribution within marine and estuarine sediments of western moreton bay, queensland, Australia: relation to land use and setting. *Geographical Res.* 43, 173–193. doi: 10.1111/j.1745-5871.2005.00312.x

Department of Environment, Science and Innovation, Queensland. (2013). *Lyngbya Monitoring Program, WetlandInfo website*, accessed 3 April 2024. Available at: https://wetlandinfo.des.qld.gov.au/wetlands/assessment/monitoring/current-and-future-monitoring/lyngbya-monitoring-program.html.

Fitzsimmons, J. N., and Conway, T. M. (2023). Novel insights into marine iron biogeochemistry from iron isotopes. *Annu. Rev. Mar. Sci.* 15, 383–406. doi: 10.1146/annurev-marine-032822-103431

Gibbes, B., Robinson, C., Carey, H., Li, L., and Lockington, D. (2008). Tidally driven pore water exchange in offshore intertidal sandbanks: Part I. Field measurements. *Estuarine Coast. Shelf Sci.* 79, 121–132. doi: 10.1016/j.ecss.2008.03.021

Gibbes, B., Robinson, C., Li, L., and Lockington, D. (2007). Measurement of hydrodynamics and pore water chemistry in intertidal groundwater systems. *J. Coast. Res.* 884–894.

Hanington, P., Rose, A., and Johnstone, R. (2016). The potential of benthic iron and phosphorus fluxes to support the growth of a bloom forming toxic cyanobacterium Lyngbya majuscula, Moreton Bay, Australia. *Mar. Freshw. Res.* 67, 1918. doi: 10.1071/MF15219

Hiemstra, T., Mendez, J. C., and Li, J. (2019). Evolution of the reactive surface area of ferrihydrite: time, pH, and temperature dependency of growth by Ostwald ripening. *Environ. Sci.: Nano* 6, 820–833. doi: 10.1039/C8EN01198B

Houben, G. J. (2003). Iron oxide incrustations in wells. Part 1: genesis, mineralogy and geochemistry. *Appl. Geochemistry* 18, 927–939. doi: 10.1016/S0883-2927(02)00242-1

Kroeger, K. D., and Charette, M. A. (2008). Nitrogen biogeochemistry of submarine groundwater discharge. *Limnol. Oceanogr* 53, 1025–1039. doi: 10.4319/lo.2008.53.3.1025

Kuan, W. K., Xin, P., Jin, G., Robinson, C. E., Gibbes, B., and Li, L. (2019). Combined effect of tides and varying inland groundwater input on flow and salinity distribution in unconfined coastal aquifers. *Water Resour. Res.* 55, 8864–8880. doi: 10.1029/2018WR024492

Kügler, S., Cooper, R. E., Wegner, C.-E., Mohr, J. F., Wichard, T., and Küsel, K. (2019). Iron-organic matter complexes accelerate microbial iron cycling in an iron-rich fen. *Sci. Total Environ.* 646, 972–988. doi: 10.1016/j.scitotenv.2018.07.258

Lalonde, K., Mucci, A., Ouellet, A., and Gélinas, Y. (2012). Preservation of organic matter in sediments promoted by iron. *Nature* 483, 198–200. doi: 10.1038/nature10855

Larrahondo, J. M., and Burns, S. E. (2014). Laboratory-prepared iron oxide coatings on sands: surface characterization and strength parameters. *J. Geotech. Geoenviron. Eng.* 140, 04013052. doi: 10.1061/(ASCE)GT.1943-5606.0001068

LePan, N., and Venditti, B. (2021) *Visualizing the Abundance of Elements in the Earth's Crust* (Elements Newsletter). Available at: https://elements.visualcapitalist.com/elements-in-the-earths-crust-abundance/.

Li, L., Barry, D. A., Stagnitti, F., and Parlange, J. Y. (1999). Submarine groundwater discharge and associated chemical input to a coastal sea. *Water Resour. Res.* 35, 3253–3259. doi: 10.1029/1999WR900189

Linkhorst, A., Dittmar, T., and Waska, H. (2017). Molecular fractionation of dissolved organic matter in a shallow subterranean estuary: the role of the iron curtain. *Environ. Sci. Technol.* 51, 1312–1320. doi: 10.1021/acs.est.6b03608

Liu, Y., Jiao, J. J., and Luo, X. (2016). Effects of inland water level oscillation on groundwater dynamics and land-sourced solute transport in a coastal aquifer. *Coast. Eng.* 114, 347–360. doi: 10.1016/j.coastaleng.2016.04.021

Liu, B., Yan, G., Ma, Y., and Scheuermann, A. (2023). Measurement of in-situ flow rate in borehole by heat pulse flowmeter: field-case study and reflection. *Geosciences* 13, 146. doi: 10.3390/geosciences13050146

Lloyd, R. R., Provis, J. L., and van Deventer, J. S. J. (2009). Microscopy and microanalysis of inorganic polymer cements. 1: remnant fly ash particles. *J. Mater Sci.* 44, 608–619. doi: 10.1007/s10853-008-3077-0

Luef, B., Fakra, S. C., Csencsits, R., Wrighton, K. C., Williams, K. H., Wilkins, M. J., et al. (2013). Iron-reducing bacteria accumulate ferric oxyhydroxide nanoparticle aggregates that may support planktonic growth. *ISME J.* 7, 338–350. doi: 10.1038/ismej.2012.103

Manson, F. J., Loneragan, N. R., and Phinn, S. R. (2003). Spatial and temporal variation in distribution of mangroves in Moreton Bay, subtropical Australia: a comparison of pattern metrics and change detection analyses based on aerial photographs. *Estuarine Coast. Shelf Sci.* 57, 653–666. doi: 10.1016/S0272-7714(02)00405-5

Martin, J. B., Hartl, K. M., Corbett, D. R., Swarzenski, P. W., and Cable, J. E. (2003). A multi-level pore-water sampler for permeable sediments. *J. Sedimentary Res.* 73, 128–132. doi: 10.1306/070802730128

McAllister, S. M., Barnett, J. M., Heiss, J. W., Findlay, A. J., MacDonald, D. J., Dow, C. L., et al. (2015). Dynamic hydrologic and biogeochemical processes drive microbially enhanced iron and sulfur cycling within the intertidal mixing zone of a beach aquifer: Fe and S cycling in a beach aquifer. *Limnol. Oceanogr.* 60, 329–345. doi: 10.1002/lno.10029

Miller, D. C., and Ullman, W. J. (2004). Ecological consequences of ground water discharge to Delaware Bay, United States. *Ground Water* 42, 959–970. doi: 10.1111/j.1745-6584.2004.tb02635.x

Mo, Y., Jin, G., Zhang, C., Xu, J., Tang, H., Shen, C., et al. (2021). Combined effect of inland groundwater input and tides on flow and salinization in the coastal reservoir and adjacent aquifer. *J. Hydrology* 600, 126575. doi: 10.1016/j.jhydrol.2021.126575

Moore, W. S. (2003). Sources and fluxes of submarine groundwater discharge delineated by radium isotopes. *Biogeochemistry* 66, 75–93. doi: 10.1023/B:BIOG.0000006065.77764.a0

O'Neil, J. M., and Dennison, W. C. (2016). "Discerning the Causes of Toxic Cyanobacteria (Lyngbya majuscula) Blooms in Moreton Bay, Australia," in *Aquatic Microbial Ecology and Biogeochemistry: A Dual Perspective*. Eds. P. M. Glibert and T. M. Kana (Springer International Publishing, Cham), 261–272. doi: 10.1007/978-3-319-30259-1_21

Paffrath, R., Pahnke, K., Behrens, M. K., Reckhardt, A., Ehlert, C., Schnetger, B., et al. (2020). Rare earth element behavior in a sandy subterranean estuary of the southern North Sea. *Front. Mar. Sci.* 7. doi: 10.3389/fmars.2020.00424

Porubsky, W. P., Weston, N. B., Moore, W. S., Ruppel, C., and Joye, S. B. (2014). Dynamics of submarine groundwater discharge and associated fluxes of dissolved nutrients, carbon, and trace gases to the coastal zone (Okatee River estuary, South Carolina). *Geochimica Cosmochimica Acta* 131, 81–97. doi: 10.1016/j.gca.2013.12.030

Reckhardt, A., Beck, M., Seidel, M., Riedel, T., Wehrmann, A., Bartholomä, A., et al. (2015). Carbon, nutrient and trace metal cycling in sandy sediments: A comparison of high-energy beaches and backbarrier tidal flats. *Estuarine Coast. Shelf Sci.* 159, 1–14. doi: 10.1016/j.ecss.2015.03.025

Reddy, K. (2000). Nitrate removal from groundwater using catalytic reduction. *Water Res.* 34, 995–1001. doi: 10.1016/S0043-1354(99)00227-4

Robinson, C., Gibbes, B., Carey, H., and Li, L. (2007). Salt-freshwater dynamics in a subterranean estuary over a spring-neap tidal cycle. *J. Geophys. Res.* 112, C09007. doi: 10.1029/2006JC003888

Robinson, C., Gibbes, B., and Li, L. (2006). Driving mechanisms for groundwater flow and salt transport in a subterranean estuary. *Geophys. Res. Lett.* 33, L03402. doi: 10.1029/2005GL025247

Robinson, C. E., Xin, P., Santos, I. R., Charette, M. A., Li, L., and Barry, D. A. (2018). Groundwater dynamics in subterranean estuaries of coastal unconfined aquifers: Controls on submarine groundwater discharge and chemical inputs to the ocean. *Adv. Water Resour.* 115, 315–331. doi: 10.1016/j.advwatres.2017.10.041

Roy, M., Martin, J. B., Cherrier, J., Cable, J. E., and Smith, C. G. (2010). Influence of sea level rise on iron diagenesis in an east Florida subterranean estuary. *Geochimica Cosmochimica Acta* 74, 5560–5573. doi: 10.1016/j.gca.2010.07.007

Russo, A. A., Boutt, D. F., Munk, L. A., and Jenckes, J. (2023). Contribution of fresh submarine groundwater discharge to the gulf of Alaska. *Water Resour. Res.* 59, e2023WR034912. doi: 10.1029/2023WR034912

Saeck, E., Grinham, A., Coates-Marnane, J., McAlister, T., and Burford, M. (2019). Primary producers in Moreton Bay: Phytoplankton, benthic microalgae and filamentous cyanobacteria. In Tibbetts, I. R., Rothlisberg, P. C., Neil, D. T., Hoburg, T. A., Brewer, D. T., and Arthington, A. H. (Editors). *Moreton Bay Quandamooka & Catchment: Past, present, and future*. The Moreton Bay Foundation (pp. 187-210). Brisbane, Australia. Available at: https://moretonbayfoundation.org/.

Santos, I. R., Burnett, W. C., Dittmar, T., Suryaputra, I. G. N. A., and Chanton, J. (2009). Tidal pumping drives nutrient and dissolved organic matter dynamics in a Gulf of Mexico subterranean estuary. *Geochimica Cosmochimica Acta* 73, 1325–1339. doi: 10.1016/j.gca.2008.11.029

Scholz, M. (2019). "Dye Wastewater Treatment by Vertical-Flow Constructed Wetlands," in *Sustainable Water Treatment* (Elsevier), 191–213. doi: 10.1016/B978-0-12-816246-0.00008-2

Sevinç Şengör, S., Spycher, N. F., Ginn, T. R., Sani, R. K., and Peyton, B. (2007). Biogeochemical reactive–diffusive transport of heavy metals in Lake Coeur d'Alene sediments. *Appl. Geochemistry* 22, 2569–2594. doi: 10.1016/j.apgeochem.2007.06.011

Shen, C., Zhang, C., Xin, P., Kong, J., and Li, L. (2018). Salt dynamics in coastal marshes: formation of hypersaline zones. *Water Resour. Res.* 54, 3259–3276. doi: 10.1029/2017WR022021

Slomp, C. P., and Van Cappellen, P. (2004). Nutrient inputs to the coastal ocean through submarine groundwater discharge: Controls and potential impact. *J. Hydrology* 295, 64–86. doi: 10.1016/j.jhydrol.2004.02.018

Spiteri, C., Regnier, P., Slomp, C. P., and Charette, M. A. (2006). pH-Dependent iron oxide precipitation in a subterranean estuary. *J. Geochemical Explor.* 88, 399–403. doi: 10.1016/j.gexplo.2005.08.084

Spiteri, C., Slomp, C. P., Tuncay, K., and Meile, C. (2008). Modeling biogeochemical processes in subterranean estuaries: Effect of flow dynamics and redox conditions on submarine groundwater discharge of nutrients: Biochemistry of subterranean estuaries. *Water Resour. Res.* 44, W02430. doi: 10.1029/2007WR006071

Sukekava, C. F., Downes, J., Filella, M., Vilanova, B., and Laglera, L. M. (2024). Ligand exchange provides new insight into the role of humic substances in the marine iron cycle. *Geochimica Cosmochimica Acta* 366, 17–30. doi: 10.1016/j.gca.2023.12.007

Testa, J. M., Charette, M. A., Sholkovitz, E. R., Allen, M. C., Rago, A., and Herbold, C. W. (2002). Dissolved iron cycling in the subterranean estuary of a coastal bay: waquoit bay, massachusetts. *Biol. Bull.* 203, 255–256. doi: 10.2307/1543427

Thamdrup, B., Finster, K., Fossing, H., Hansen, J. W., and Jørgensen, B. B. (1994). Thiosulfate and sulfite distributions in porewater of marine sediments related to manganese, iron, and sulfur geochemistry. *Geochimica Cosmochimica Acta* 58, 67–73. doi: 10.1016/0016-7037(94)90446-4

Ullman, W. J., Chang, B., Miller, D. C., and Madsen, J. A. (2003). Groundwater mixing, nutrient diagenesis, and discharges across a sandy beachface, Cape Henlopen, Delaware (USA). *Estuarine Coast. Shelf Sci.* 57, 539–552. doi: 10.1016/S0272-7714(02)00398-0

Van Der Grift, B., Behrends, T., Osté, L. A., Schot, P. P., Wassen, M. J., and Griffioen, J. (2016). Fe hydroxyphosphate precipitation and Fe(II) oxidation kinetics upon aeration of Fe(II) and phosphate-containing synthetic and natural solutions. *Geochimica Cosmochimica Acta* 186, 71–90. doi: 10.1016/j.gca.2016.04.035

Viscarra Rossel, R. A., Bui, E. N., de Caritat, P., and McKenzie, N. J. (2010). Mapping iron oxides and the color of Australian soil using visible–near-infrared reflectance spectra. *J. Geophys. Res.* 115, F04031. doi: 10.1029/2009JF001645

Wu, Z., Wang, S., and Ji, N. (2019). Distribution character of localized iron microniche in lake sediment microzone revealed by chemical image. *Environ. Sci. pollut. Res.* 26, 35704–35716. doi: 10.1007/s11356-019-06219-2

Xin, P., Robinson, C., Li, L., Barry, D. A., and Bakhtyar, R. (2010). Effects of wave forcing on a subterranean estuary. *Water Resour. Res.* 46, W12505. doi: 10.1029/2010WR009632

Yan, G., Ma, Y., Scheuermann, A., and Li, L. (2022a). The hydraulic properties of aquabeads considering forchheimer flow and local heterogeneity. *Geotech. Test. J.* 45, 20210234. doi: 10.1520/GTJ20210234

Yan, G., Shi, H., Ma, Y., Scheuermann, A., and Li, L. (2022b). Intrinsic permeabilities of transparent soil under various aqueous environmental conditions. *Géotechnique Lett.* 12, 225–231. doi: 10.1680/jgele.22.00049

Zhang, J., Zhu, X., Zhang, R., Ren, J., Wu, Y., Liu, S., et al. (2022). Dissolved fe in the east China sea under the influences of land sources and the boundary current with implications for global marginal seas. *Global Biogeochemical Cycles* 36, e2021GB006946. doi: 10.1029/2021GB006946

Zhou, S., Chen, S., Yuan, Y., and Lu, Q. (2015). Influence of humic acid complexation with metal ions on extracellular electron transfer activity. *Sci. Rep.* 5, 17067. doi: 10.1038/srep17067

Zipperle, A., and Reise, K. (2005). Freshwater springs on intertidal sand flats cause a switch in dominance among polychaete worms. *J. Sea Res.* 54, 143–150. doi: 10.1016/j.seares.2005.01.003